CHEMISTRY OF MATERIALS
Article

Chem. Mater. **2010,** *22,* 3807–3816 3807
DOI:10.1021/cm100571v

Spin-Flop Transition and Magnetocaloric Effect through Disconnected Magnetic Blocks in Co^{III}/Co^{IV} Oxybromides

Olivier Toulemonde,[†] Pascal Roussel,[‡] Olivier Isnard,[§] Gilles André,[∥] and Olivier Mentré*[,‡]

[†]*CNRS, Université de Bordeaux, ICMCB, 87 avenue du Dr. A. Schweitzer, Pessac, F-33608, France,* [‡]*Unité de Catalyse et de Chimie du Solide, UCCS−Equipe de Chimie du Solide-UMR 8181, bât. C7, BP 90108, 59655 Villeneuve d' Ascq cedex, France,* [§]*Institut Néel du CNRS/Université Joseph Fourier, Département MCMF, BP166X, F-38042 Grenoble Cédex 9, France, and* [∥]*Laboratoire Léon Brillouin CEA Saclay, bât.563, 91191, Gif-sur-Yvette cedex, France*

Received February 24, 2010. Revised Manuscript Received May 4, 2010

The magnetic properties of the layered $Ba_{n+1}Co_nO_{3n-1}Br$ ($n = 5$ and 6) oxybromides have been determined by means of magnetization measurements and neutron diffraction under variable magnetic field. For $n = 6$, the magnetic phase diagram has been built on the basis of several features, including the notions of short-range ordering, spin reorientation, and spin-flop transitions. In those compounds, the competition between magnetic exchanges arise from the existence of $[Ba_2O_2Br]^-$ double-layers that separate perovskite 2D-blocks. The latter are dominated by ferromagnetic (FM) intraexchanges while the interblock exchanges are antiferromagnetic (AFM). Interestingly, a perturbation created by an external magnetic field could be on the same order of magnitude than the interblock exchange leading to a complex set of spin reorientations versus H and T. From the point of view of magneto-crystalline anisotropy, the AFM system with moments parallel to the c-axis turns into a FM system with moments aligned in the perpendicular (a,b) planes. The magnetic entropy is distributed within at least three phenomena, spread out in a wide range of temperature. Here, the influence of the magneto-crystalline anisotropy on the magnetocaloric effect is unambiguously shown.

I. Introduction

Nowadays, the need for low cost energy stimulates the development of better-adapted prototypes and/or the research of new energy sources. Among them, extensive studies about the magnetocaloric effect (MCE) are being carried out since the discovery of a giant magnetocaloric effect in $Gd_5(Si_xGe_{1-x})_4$.[1] The MCE is characterized by a temperature change of a magnetic material under an applied magnetic field[2] and is believed to be a good alternative for magnetic cooling units in the future.[3] In that frame, a large class of materials have been studied, including intermetallics La−Fe−Si and Gd−Si−Ge series, Mn/Fe-based arsenic materials and manganite compounds.[4−6] To our knowledge, the largest MCE has been found in the compound $Mn_{1.1}Fe_{0.9}P_{0.8}Ge_{0.2}$ with 74 J/kg K around 255 K.[7]

Quantitatively, from thermodynamics and using the Maxwell formalism, the isothermal field-induced magnetic entropy change from 0 to H can be written as[8]

$$\Delta S_M(T,H) = \int_0^H \frac{\delta M}{\delta T}\,\partial H \qquad (1)$$

Determining the field-induced isothermal specific heat change, the field-induced adiabatic temperature change (ΔT_{ad}) at the magnetic transition from 0 to H can be evaluated by

$$\Delta T_{ad} = -\int_0^H \frac{T}{C_{P,H}}\left(\frac{\partial M}{\partial T}\right)\partial H \qquad (2)$$

Thus, there is an immediate correlation between the sign of the magnetic entropy change and the capability of the concerned compound to be used as a cooling or heating medium. Such opposite behaviors are referred as inverse or normal MCE, respectively, and are usually associated with antiparallel or parallel spin arrangements. More recently, a quantitative parameter expected

*To whom correspondence should be addressed. E-mail: olivier.mentre@ensc-lille.fr.

(1) Pecharsky, V. K.; Gschneider, K. A., Jr. *Phys. Rev. Lett.* **1997**, *78*, 4494.
(2) Warburg, E. *Ann. Phys.* **1881**, *13*, 141.
(3) Gschneidner, K. A., Jr.; Pecharsky, V. K. *Int. J. Refrig.* **2008**, *31*, 945.
(4) Brück, E.; Tegus, O.; Cam Thanh, D. T.; Trung, N. T.; Buschow, K. H. J. *Int. J. Refrig.* **2008**, *31*, 763.
(5) Gschneidner, A., Jr.; Pecharsky, V. K.; Tsokol, A. O. *Rep. Prog. Phys.* **2005**, *68*, 1479.
(6) M.-H. Phana, M.-H.; Yu, S.-C. *J. Magn. Magn. Mater.* **2007**, *308*, 325.
(7) Liu, D.; Yue, M.; Zhang, J.; Mc Queen, T. M.; Lynn, J. W.; Wang, X.; Chen, Y.; Li, J.; Cava, R. J.; Liu, X.; Altounian, Z.; Huang, Q. *Phys. Rev. B* **2009**, *79*, 014435.
(8) Tishin, A. M. Spichkin, Y. I. *The Magnetocaloric Effect and its Applications*; Institute of Physics Publishing: Bristol, 2003.

Published on Web 05/28/2010

to be suitable for application has been introduced: the Relative Cooling (or Heating) Power, hereafter RCP.[8] For instance, in the case of a refrigerator describing a thermodynamic cycle, it would indicate how much heat can be transferred from the cold to the hot end. It can be estimated by the product $\Delta S_M(T)^{max} \times \delta T_{fwhm}$ where δT_{fwhm} is the full width at half-maximum of the field induced magnetic entropy change $\Delta S_M(T)$. The refrigerant capacity in the appropriate temperature span is given by the following integration

$$Q = \int_{T1}^{T2} \Delta S_M(T,H) \partial T \quad (3)$$

Up to now, further routes are being investigated to find new materials showing giant MCE and/or RCP as high as possible. One possible way to enlarge the RCP is to elaborate materials showing multiple magnetic transitions.[9] In the present paper, we suggest another route, taking advantage of the possible tuning of the magnetocrystalline anisotropy as already proposed by Isnard et al.[10] We report herein the fine magnetic investigation of the 18R-$Ba_6Co_5BrO_{14-\delta}$ and 14H-$Ba_7Co_6BrO_{17-\delta}$ compounds[11] which belong to a series of hexagonal perovskite compounds recently isolated in the Ba−Co−O−X chemical systems (X = F, Cl, Br).[12] Those compounds show disconnected 2D-blocks at both sides of central $[Ba_2O_2Br]$ double-layers. They can also be described as $n = 5$ and $n = 6$ members of the series $Ba_{n+1}Co_nO_{3n-1}Br$, underlying the layered aspect of the compounds. This topology is such that the nature of the exchanges between the blocks and the magneto-crystalline anisotropy is strongly depending on the applied magnetic field. Strikingly, an external field promotes spin-flop and spin reorientation transitions which leads (i) to enlarge the full width at half-maximum of $\Delta S(T)$ and then the refrigerant capacity and (ii) to tune the sign of the magnetic entropy. It follows that those compounds could be considered as cooling or heating media at constant temperature depending on the amplitude of the applied magnetic field.

II. Experimental Procedures

Neutron Diffraction. Pure powder of $Ba_{n+1}Co_nO_{3n-1}Br$ ($n = 5$ and 6) compounds have been prepared as described in a previous work dedicated to the crystal structure of those recent compounds.[11] Their magnetic structures versus temperature, at zero field, have been refined from neutron diffraction (ND) data collected on the G4.1 diffractometer, $\lambda = 2.425$ Å (LLB, Saclay, France). The influence of an applied field has been investigated through different ND data sets collected at the high flux D1B diffractometer, $\lambda = 2.52$ Å (ILL, Grenoble France). In a first experiment, an electromagnet with $H < 1.2$ T was used on free powder. In a subsequent stage, we benefited from a cryo-magnet with H going up to 2.5 T, which was used on dense pellets. In both cases, the applied magnetic field was oriented vertically, that is, perpendicular to the scattering vector. The temperature and applied field have been varied from 1.4 K to 90 K and from 0 to 2.5 T, respectively.

Magnetic Measurements. Magnetization experiments have been performed using a Superconducting Quantum Interference Device (SQUID, Quantum Design) under a direct current (dc) field. For both temperature and field dependence studies, the sample was introduced at room temperature and cooled down in zero-field at 5 K/min before the magnetic field was applied. $M(T)$ measurements were performed on warming the sample. The magnetic hysteresis loops were alternatively measured by increasing and decreasing the applied magnetic field.

III. Structural Aspects of the Related Series of Compounds

Starting from the 1D 2H-$BaCoO_3$ with isolated columns of face-sharing CoO_6 containing low spin (LS) Co^{IV}, $S = 1/2$[12,13] the introduction of oxygen deficient $[BaO_2]^{2-}$ layers yields the two 5H- and 12H-$BaCoO_{3-\delta}$ polymorphs, that is, $BaCoO_{2.74}$ and $BaCoO_{2.6}$ respectively. They are formed of face sharing octahedral oligomers, namely trimeric-$[Co_3O_{12}]_{5H}$ or tetrameric-$[Co_4O_{15}]_{12H,}$ capped by terminal CoO_4 tetrahedra.[14−16] In the $BaCoO_{3-\delta}$ polytypes, the so-formed 2D-blocks are not connected by their terminal tetrahedra. The replacement of the central deficient $[BaO_2]^{2-}$ layers by either $[BaOX]^-$ layers (X = F, Cl)[12,17−20] or $[Ba_2O_2Br]^-$ double-layers[11] enables various connections between the common 2D-blocks. See ref. 12 for a review on the preliminary electric and magnetic investigations. In the title compounds $Ba_6Co_5BrO_{14-\delta}$ (a = 5.6578(3) Å, c = 43.166(4), space group $R\bar{3}m$) and $Ba_7Co_6BrO_{17-\delta}$ (a = 5.666(1) Å, c = 33.367(2) Å, space group $P6_3/mmc$), the trimeric and tetrameric 2D-blocks, are respectively pushed aside the c-axis and shifted in the (a,b) plane because of the central $[Ba_2O_2Br]^-$ double layer, see Figure1a-b. On this figure are also shown individual 5H- and 6H-blocks.

IV. Magnetic Ordering at Zero-Field

The preliminary magnetic characterizations of the two compounds are shown on the Figure 2. This figure emphasizes their similar behaviors. From the $M(T)/H$ plots measured for an applied field $H = 1$ T, the characteristics of the paramagnetic domains have been extracted from the typical Curie−Weiss behavior at high temperature, that is, $Ba_7Co_6BrO_{17-\delta}$: $\mu_{eff} = 3.12\ \mu_B$/Co and $\theta_{CW} = 48.7$ K ; $Ba_6Co_5BrO_{14-\delta}$: $\mu_{eff} = 3.56\ \mu_B$/Co and $\theta_{CW} = 45.1$ K. The values of θ_{CW}, close to those found for other hexagonal cobaltites,[22,23] emphasize the similarity existing in this class of

(9) Gorsse, S.; Chevalier, B.; Orveillon, G. *Appl. Phys. Lett.* **2008**, *92*, 122501.
(10) Isnard, O.; Pop, V.; Toussaint, J. C.; Buschow, K. H. J. *J. Magn. Magn. Mater.* **2004**, *272−276*, e335–e336.
(11) Kauffmann, M.; Roussel, P. *Acta Crystallogr. B* **2007**, *63*, 589.
(12) Mentré, O.; Kauffmann, M.; Ehora, G.; Daviero-Minaud, S.; Abraham, F.; Roussel, P. *Solid State Sci.* **2008**, *10*, 471.
(13) Pardo, V.; Blaha, P.; Iglesias, M.; Schwarz, K.; Baldomir, D.; Arias, J. E. *Phys. Rev. B* **2004**, *70*, 144422.
(14) Yamaura, K.; Cava, R. J. *Solid State Commun.* **2000**, *115*, 301.
(15) Jacobson, A. J.; Hutchison, J. L. *J. Solid State Chem.* **1980**, *35*, 334.
(16) Parras, M.; Varela, Aa.; Seehofer, H.; Gonzalez-Calbet, J. M. *J. Solid State, Chem.* **1995**, *120*, 327.
(17) Darriet, J.; Subramaniam, M. A. *J. Mater. Chem.* **1995**, *5*, 543.
(18) Yamaura, K.; Young, D. P.; Siegrist, T.; Besnard, C.; Svensson, C.; Liu, Y.; Cava, R. J. *J. Solid State Chem.* **2001**, *158*, 175.
(19) Tancret, N.; Roussel, P.; Abraham, F. *J. Solid State Chem.* **2005**, *178*, 3066.
(20) Ehora, G.; Renard, C.; Daviero-Minaud, S.; Mentré, O. *Chem. Mater.* **2007**, *19*, 2924.
(21) Kauffmann, M.; Mentré, O.; Legris, A.; Tancret, N.; Abraham, F.; Roussel, P. *Chem. Phys. Lett.* **2006**, *432*, 88.
(22) Boulahya, K.; Parras, M.; González-Calbet, J. M.; Amador, U.; Martínez, J. L.; Tissen, V.; Fernández-Díaz, M. T. *Phys. Rev. B* **2005**, *71*, 144402.

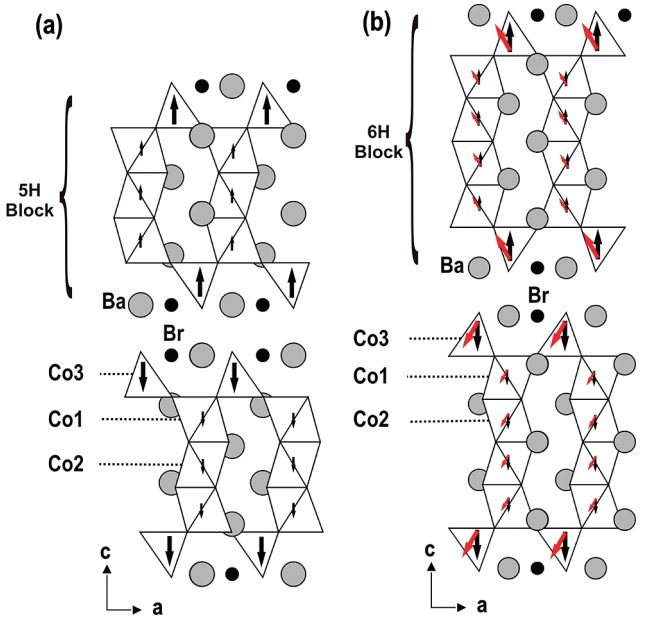

Figure 1. Crystal and magnetic structure under zero magnetic fields for (a) $Ba_6Co_5BrO_{14-\delta}$; (b) $Ba_7Co_6BrO_{17-\delta}$. In red are shown the magnetic moments refined for an applied field.

materials. As for the $BaCoO_{3-\delta}$ oxides, the positive values of θ_{CW} show dominating ferromagnetic (FM) exchanges. However, for both the $n = 5$ and 6 title compounds, an antiferromagnetic (AFM) ordering exists below $T_N \sim 50$ K. On further cooling, an additional transition occurs characterized by an abrupt increasing of M/H. This transition takes place at $T_t \sim 20$ K for both compounds and will be assigned later to spin-reorientation. For the two compounds, the $M(H)$ plots show strong field and temperature dependences (Figure2.c-d) which is the basis of our interest.

The magnetic structures refined at 1.4 K have already been shortly reported in a previous work[12] which corresponds to the moments pictured in the Figure 1. We have reinvestigated the neutron diffraction data, not only at 1.4 K, but also as a function of the temperature. In $Ba_6Co_5BrO_{14-\delta}$ ($n = 5$) magnetic satellites appear below 50 K in good agreement with the susceptibility data. They can be indexed using the propagation vector $k = (0,0,1/2)$ which corresponds to the setting of an AFM ordering between FM 2D-blocks. The local moments are lying parallel to the c-axis. At 1.4 K our refinement leads to $M(Co)_{tetra} = 3.25(5)\mu_B$, $M(Co)_{central\ octa} = 0.87(9)\mu_B$ and $M(Co)_{edge\ octa} = 0.61(6)\mu_B$ with final $R_{magn} = 5.8\%$ for $Ba_6Co_5BrO_{14-\delta}$. In $Ba_7Co_6BrO_{17-\delta}$ ($n = 6$), since the crystal-unit cell contains two blocks, the magnetic contributions are superimposed to nuclear ones, and no extra-peak grow up (propagation vector $k = (0,0,0)$). The magnetic ordering is similar for $n = 5$ and $n = 6$. The refinement at 1.4 K leads to $M(Co)_{tetra} = 3.22(5)\mu_B$, $M(Co)_{central\ octa} = 0.57(9)\mu_B$ and $M(Co)_{edge\ octa} = 0.51(6)\mu_B$ with final $R_{magn} = 4.9\%$. The experimental and calculated patterns for the two compounds are shown on the Figure 3.a-b. In fact, the assignment of the cobalt valence states in the series of related compounds has already been intensively discussed[20,21,24] suggesting octahedral Co^{III} and tetrahedral Co^{IV} in an intermediate spin state. However, this last point is contested by some recent density functional theory (DFT) calculations on oxo-fluorides containing same structural blocks which unambiguously lead to high spin (HS) Co^{III}, $S = 2$ in the tetrahedra and a mixture of low-spin (LS-) Co^{III} ($S = 0$) and LS-Co^{IV} ($S = 1/2$) in the face sharing octahedra.[25] The similitude between the individual blocks and their internal ferromagnetic ordering suggests an identical distribution in the oxo-bromides. This is also consistent with the refined values of the local moments, as the experimental μ_{eff} values match rather well this model, that is,

$$Ba_6Co_5^{+3.4}BrO_{14} : 2HS\text{-}Co^{III} + 1LS\text{-}Co^{III} + 2LS\text{-}Co^{IV}$$
$$\mu_{eff\ exp.} = 3.56\,\mu_B/Co \text{ and}$$
$$\mu_{eff\ calc./Co} = 1/\sqrt{5}\mu_{eff\ calc./f.u.} = 3.28\,\mu_B/Co$$

$$Ba_7Co_6^{+3.5}BrO_{17} : 2HS\text{-}Co^{III} + 1LS\text{-}Co^{III} + 3LS\text{-}Co^{IV}$$
$$\mu_{eff\ exp.} = 3.12\,\mu_B/Co \text{ and}$$
$$\mu_{eff\ calc./Co} = 1/\sqrt{6}\mu_{eff\ calc./f.u.} = 2.91\,\mu_B/Co$$

Note that, the calculated values respect a spin-only picture ($g = 2$). However, we cannot exclude the contribution of oxygen vacancies which would lead to significant change in the octahedral Co^{3+}/Co^{4+} partition. Furthermore, one should also take into account a significant amount of orbital contribution for cobalt cations probably responsible for the slightly underestimated calculated μ_{eff}.

The evolution of the moments versus the temperature is shown on the Figure 4.a-b for $Ba_7Co_6BrO_{17-\delta}$ and $Ba_6Co_5BrO_{14-\delta}$. For the two compounds, the moments are rapidly increasing below T_N. The magnetic moment of Co1 and Co2 refer to those of the Co atoms on the face sharing octahedra (see Figure 1). They are in good agreement with the distribution proposed from the Curie–Weiss law and suggest a delocalized spin density within the trimeric-$[Co_3O_{12}]_{5H}$ or tetrameric-$[Co_4O_{15}]_{12H}$ species assorted with direct Co–Co hybridization. Most of the magnetic moment is carried by Co3 on tetrahedral environment as illustrated on Figure 1. In fact, a fine examination of the intensities of some magnetic satellites displays an unexpected decrease below ~10 K, see Figure 5. It yields slight anomalies in the evolution of the moments at low temperature as seen on the Figure 4. This phenomenon may be correlated with the opening of a $M(H)$ hysteresis loop at low temperatures as discussed latter. However, these phenomena are relatively weak in the absence of an applied field, and ND intensities do not show the appearance of extra magnetic satellites. It is such

(23) Hebert, V.; Pralong, D.; Pelloquin; Maignan, A. *J. Magn. Magn. Mater.* **2007**, *316*, 394.
(24) Kauffmann, M.; Mentré, O.; Legris, A.; Hébert, S.; Pautrat, A.; Roussel, P. *Chem. Mater.* **2008**, *20*, 1741–1749.
(25) Mentré, O.; Kabbour, H.; Ehora, G.; Tricot, G.; Daviero-Minaud, S.; Whangbo, M.-H. *J. Am. Chem. Soc.* **2010**, *132* (13), 4865.

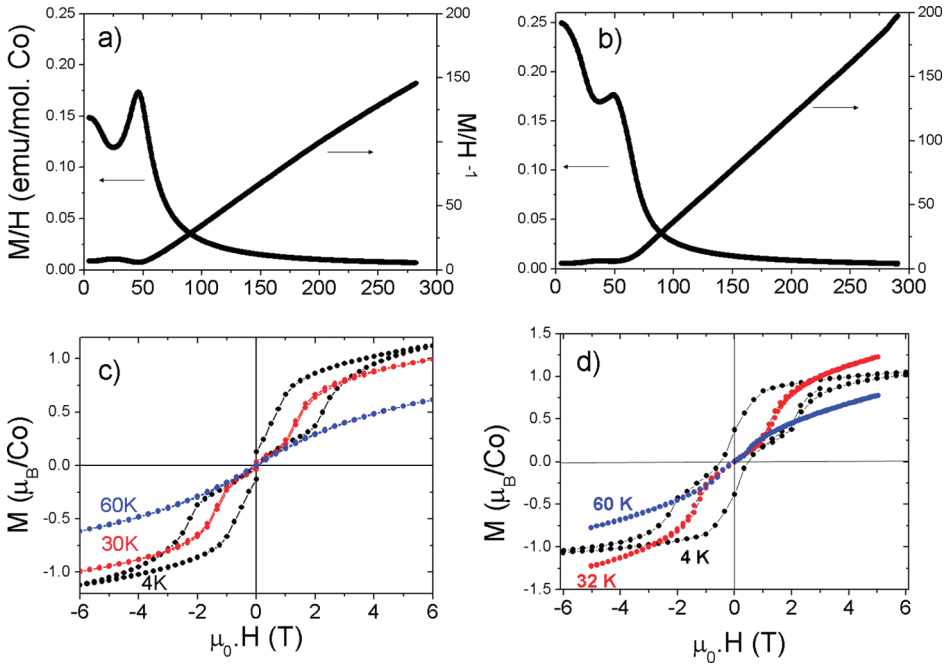

Figure 2. (a) Temperature dependence of the normalized Magnetization measured under 1 T for $Ba_6Co_5BrO_{14-\delta}$. (b) Temperature dependence of the normalized magnetization measured under 1 T for $Ba_7Co_6BrO_{17-\delta}$. (c) Isothermal magnetization versus magnetic field at the indicated temperature for $Ba_6Co_5BrO_{14-\delta}$. (d) Isothermal magnetization versus magnetic field at the indicated temperature for $Ba_7Co_6BrO_{17-\delta}$.

that in the Rietveld refinements, our attempts to deviate the moments out of the *c*-axis failed in the absence of an external field. As we will see in the next section, the concerned spin reorientation will be best characterized under an applied magnetic field.

V. Effect of an Applied Field

The linear increase of the magnetization plots observed in the Figure 2 for the two compounds under low applied field reveals AFM ordering below T_N consistent with the magnetic ground state previously discussed. The magnetization curves deviate from this linear behavior under high magnetic field indicating a field induced metamagnetic transition from AFM to FM states as supported by the opening of the magnetic hysteresis. Such metamagnetism is likely associated in those systems with the strong disconnection between the blocks. The topology of the two compounds is such that the AFM interblock exchanges are weakest compared to related "*tetrahedra-connected*" systems. It was attempted to clarify the existence of such metamagnetic transition using ND. Precisely, our main goal is to distinguish between two possible magnetic configurations that could occur under an external magnetic field: (1) the progressive reversal of magnetic moments, conserving their orientation parallel to *c*. This would involve the setting of variable ferrimagnetic ordering until the FM saturation; (2) an increasing tilt of the spins leading to canted structures leading to a magnetic contribution parallel to the (*a*,*b*) planes. The evolution of the ND-magnetic lines or the appearance of a new magnetic peak should give clear indications on the magnitude and direction of the moments versus *H*. The first collected data sets using free-powder of $Ba_7Co_6BrO_{17-\delta}$ sample below T_N is shown on Figure 6. A strong reorientation of the crystallites is observed for applied fields greater than 0.5 T. It is evidenced by a strong modification of the full diffraction pattern, that is, strong decrease of I_{00l}, strong increase of the I_{hk0}, and variable behavior of I_{h0l} depending on the h/l ratio. It pictures a drastic reorientation of the crystallites because of the alignment of the induced ferromagnetic component parallel to the vertical applied field. Most of the crystals are now reoriented with *hk*0 faces parallel to the applied field (i.e., in favor of *hk*0 diffraction) and suggests the occurrence of the canted structure according to the above-model 2 (i.e., with a magnetic component in the (*a*,*b*) plane). Indeed, in an AFM structure the magnetization is larger when applying the field perpendicularly to the direction of the moments since a low-tilt of the moments can lead a FM component.

To lock the crystallite reorientation, we decided to use, instead of free powder, some sintered pellets. However, we could not obtain dense pellets of the tetrameric $Ba_7Co_6BrO_{17-\delta}$ ($n = 6$) since it transforms into the trimeric $Ba_6Co_5BrO_{14-\delta}$ ($n = 5$) above 990 °C.[11] Then, only dense cylinders of the latter ($n = 5$) compound (compacity greater than 80%) have been used for ND experiments under applied field. As expected, in that case the reorientation of the crystallites is blocked. At 1.4 K, the evolution of the ND patterns varying *H* from 0 to 2.5 T is shown on the Figure 7. The intensities of the AFM satellites, for example, $h00 + k$, with $k = (0,0, 1/2)$ progressively decrease above $\mu_0 H = 1.2\ T$ while extra magnetic components are growing superposed to some Bragg diffraction lines, for example, the 104 and 105 peaks. They highlight a deviation of the moments away from the *c* axis. Several magnetic models have been tested by Rietveld refinement to characterize the nature of the

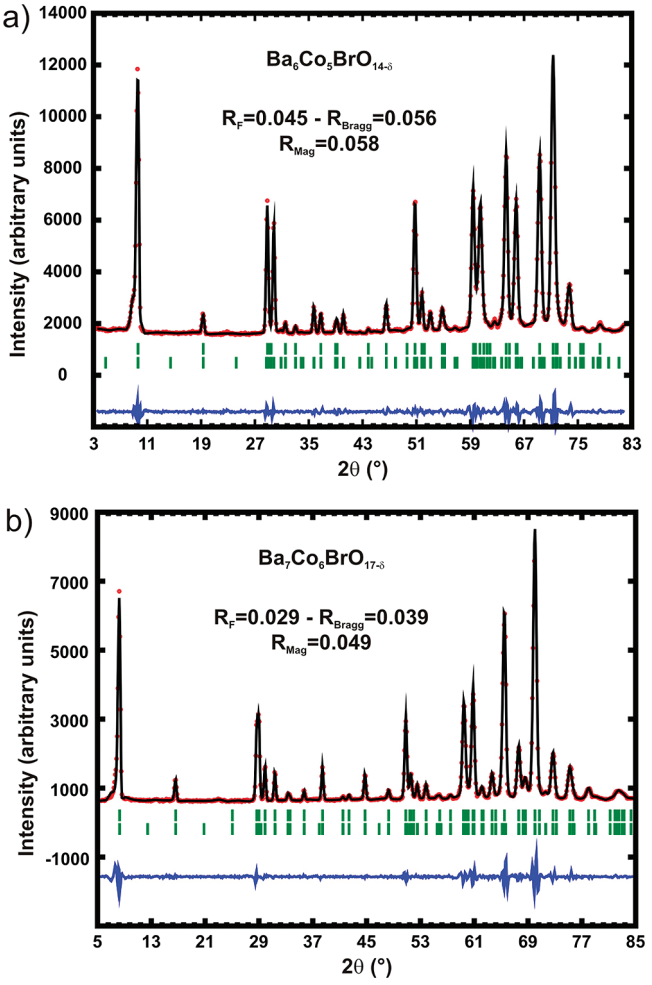

Figure 3. Experimental and calculated neutron diffraction patterns at 1.4 K (G4.1, LLB, $\lambda = 2.425$ Å) for (a) $Ba_6Co_5BrO_{14-\delta}$; (b) $Ba_7Co_6BrO_{17-\delta}$. The vertical bars indicate calculated Bragg peak positions for both nuclear (first row) and magnetic structures (second row).

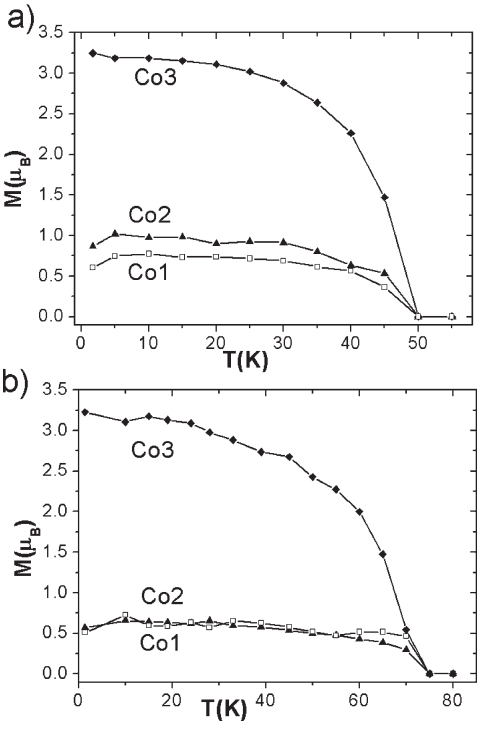

Figure 4. Thermal evolution of the magnetic moments per cobalt atom for (a) $Ba_6Co_5BrO_{14-\delta}$; (b) $Ba_7Co_6BrO_{17-\delta}$. The values were obtained from neutron diffraction data Rietveld refinement recorded on G4.1 line (LLB, Saclay).

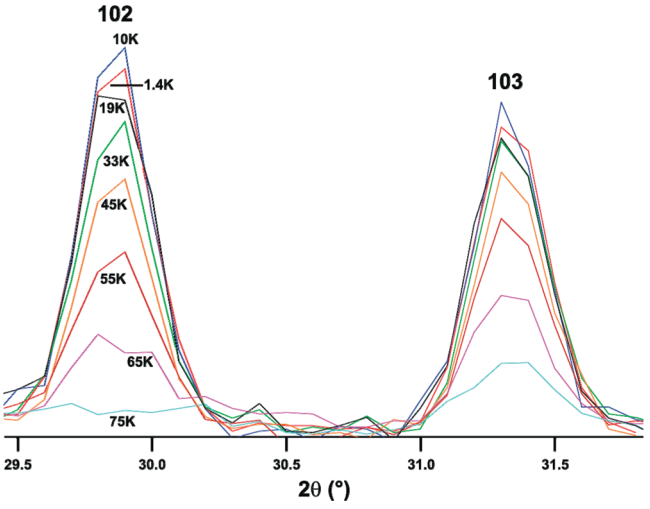

Figure 5. Temperature evolution of selected magnetic diffraction peaks for $Ba_7Co_6BrO_{17-\delta}$. Note that intensity at 10 K is higher than at 1.4 K.

spin-deviation. Actually, a canting structure from block to block leads to the best agreement (see Figure 1b). Here, to properly describe the magnetic structure, it was not possible anymore to use a propagation vector since the reversal of the moment by the (0,0,1/2) translation is not respected in the canted structure. Thus, the unit cell was doubled and each magnetic atom was introduced in association with its moment $M_{Co1\ to\ Co3}$ and a tilting angle θ or $-\theta$ from the c-axis. These models have converged leading to the best match between the experimental and calculated data, and to the successful generation of the field-induced-FM peaks while reducing AFM satellites. Depending on the value of H, the final magnetic R_F factors are between ~5 and ~10%. The M-Co(H) and $\theta(H)$ are shown on the Figure 8. Strikingly, θ reaches 42° at 2.5 T. The progressive spin-deviation is accompanied by a slight exaltation of the magnetic moments of the octahedral Co1 and Co2 and a small reduction of those on the tetrahedral Co3. Note that the slight differences in the refined moments at $\mu_0 H = 0T$ and $T = 1.4$ K between the experiments performed at D1B, ILL (i.e., with cryo-magnet), and at G4.1, LLB (i.e., without cryo-magnet), 2.79(3) μ_{B-D1b-} compared to 3.26(5) $\mu_{B\text{-}G4.1}$, can be attributed to the most narrow resolution range in the former because of the use of this cryo-magnet which unfortunately brings parasitic lines for $d_{hkl} > 2.58$ Å. However, the main picture of the magnetic structure remains identical.

VI. Spin Flop Transition

In this section we will examine in detail the magnetization of the tetrameric compound, $Ba_7Co_6BrO_{17-\delta}$, on the basis of the previously refined magnetic structures. Once more, it is clear from the Figure 2 that phenomena occurring in this compound should be also qualitatively suitable for the parent trimeric $Ba_6Co_5BrO_{14-\delta}$. Figure 9

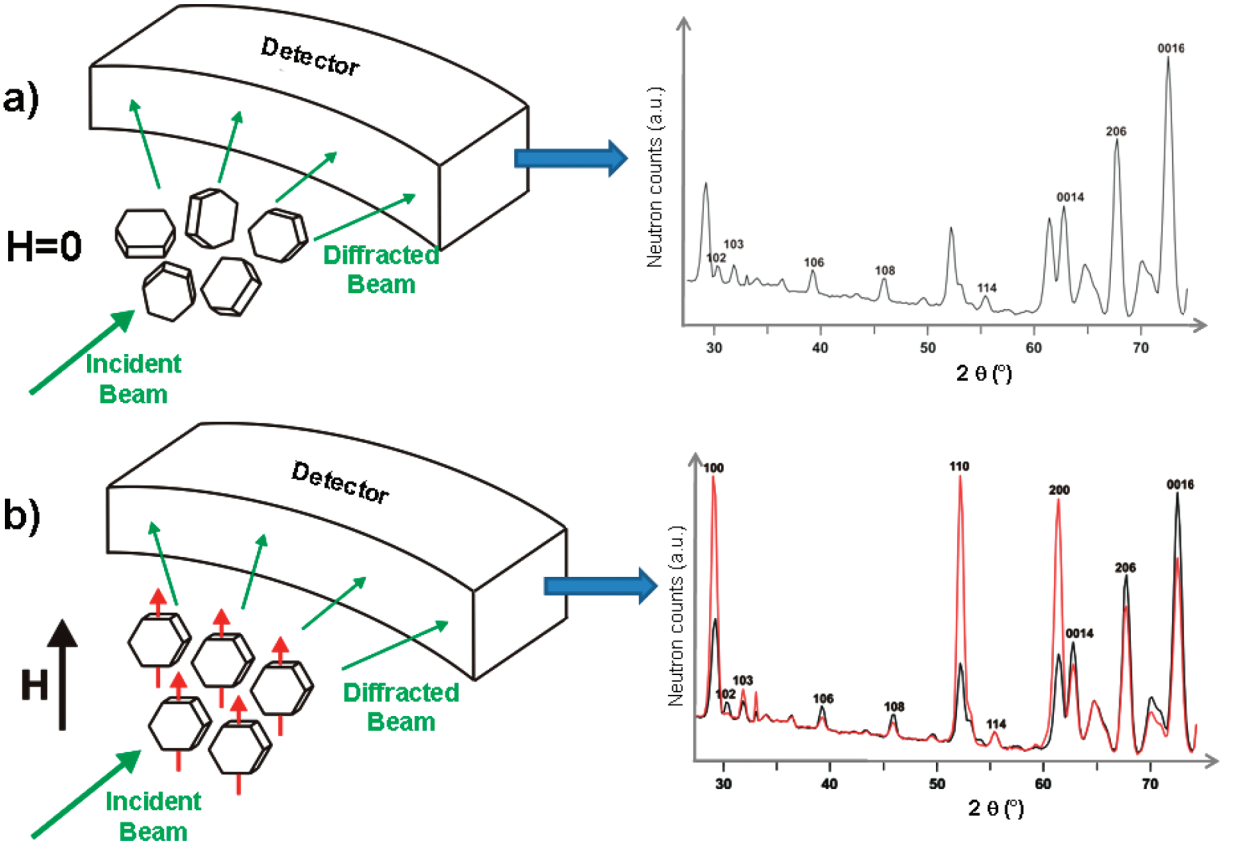

Figure 6. Neutron diffraction pattern of a non-densified powder sample of $Ba_7Co_6BrO_{17-\delta}$ at $\lambda = 2.52$ Å (a) without magnetic field; (b) with $\mu_0 H = 1.2$ *T*. The magnetic field clearly induces preferential orientations. The rotation of crystals around the magnetic easy axis (red arrows) is free.

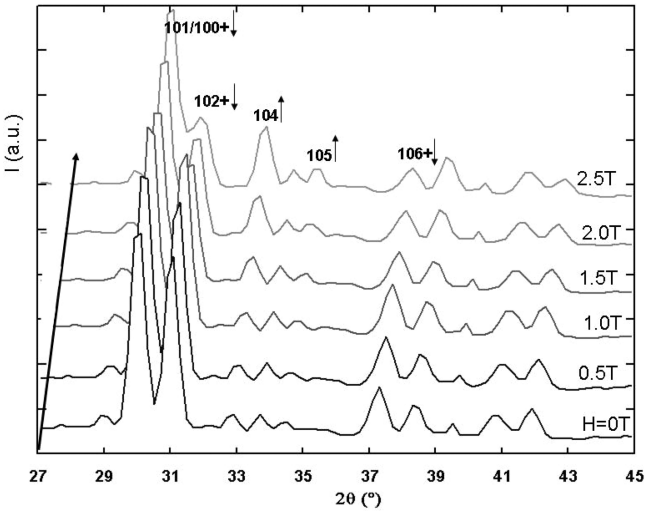

Figure 7. Evolution of the neutron diffraction pattern with the magnetic field for $Ba_7Co_6BrO_{17-\delta}$. The data were measured on the D1B line (ILL, Grenoble) equipped with a cryomagnet allowing field variation from 0 to 2.5 T.

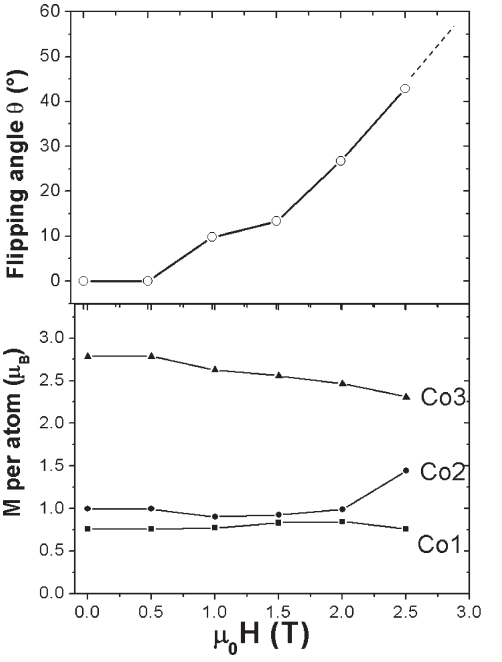

Figure 8. Evolution of the magnetic moment held per cobalt atom (bottom) and of the flipping angle for $Ba_7Co_6BrO_{17-\delta}$. The values were obtained from neutron diffraction data Rietveld refinement recorded on D1B line (ILL, Grenoble) equipped with a cryomagnet allowing field variation from 0 to 2.5 T.

represents the Zero Field-cooled $M(T)/H$ for $Ba_7Co_6BrO_{17-\delta}$ under variable field. It enhances its strong field dependence. Under 0.9 T, we recognize the two maxima briefly discussed for both compounds in the section IV.

(i) The first one centered at $T = 56$ K corresponds to the Néel temperature and corresponds to the neutron diffraction experiment. However, it displays a large broadening when the field increases until it almost vanishes (but is still observed on the derivative $dM/dT(T)$ curve at 60 K). Thus, even at T_N, an applied external field induces the setting of

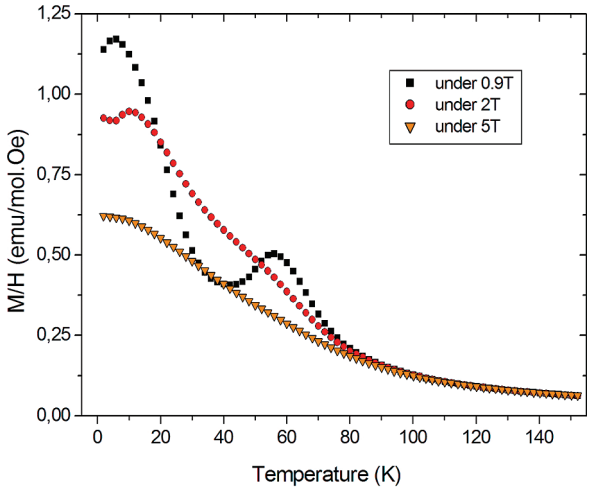

Figure 9. Temperature dependence of the normalized magnetization measured under different field for $Ba_7Co_6BrO_{17-\delta}$.

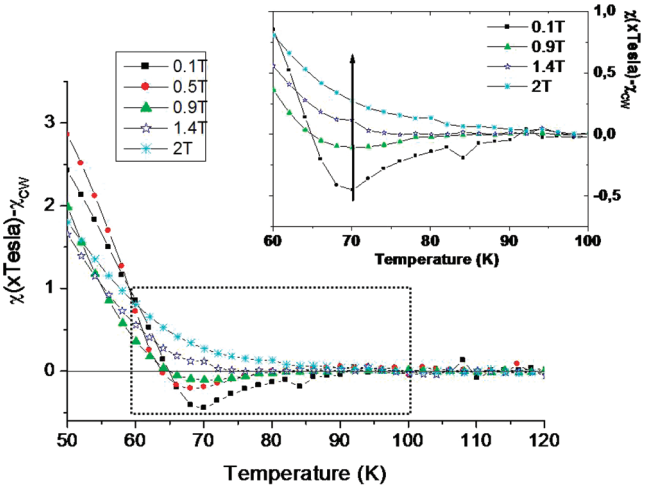

Figure 10. $Ba_7Co_6BrO_{17-\delta}$: $M(T)/H$ curves under different fields corrected from the Curie−Weiss Law susceptibility extracted on the lower temperature range. The inset show a magnification of the curve in the region near the ordering temperature. The arrow points out the change in sign observed when the applied field increases.

magnetic reorientations. Above T_N, $M(T)/H$ corrected from the Curie−Weiss susceptibility changes its sign within a critical field range between 0.9 T and 1.4 T (Figure 10). It involves a drastic change of the magnetic correlations from antiparallel to parallel alignment when H increases.

(ii) The second transition is centered at 22 K for $\mu_0 H = 0.9$ T. As shown by ND, it corresponds to the appearance of resulting ferromagnetic component in the (a,b) plane by canting. On increasing H, this transition can also be followed by the position of the local minimum of the $dM/dT(T)$ derivative curve. The transition temperature increases continuously with the field, until being equal to 30 K at 5 T. At high fields, FM exchanges predominate.

At this stage of the discussion, from the Zero Field Cooled $M(T)/H$ measurements, two kinds of ordering are observed:

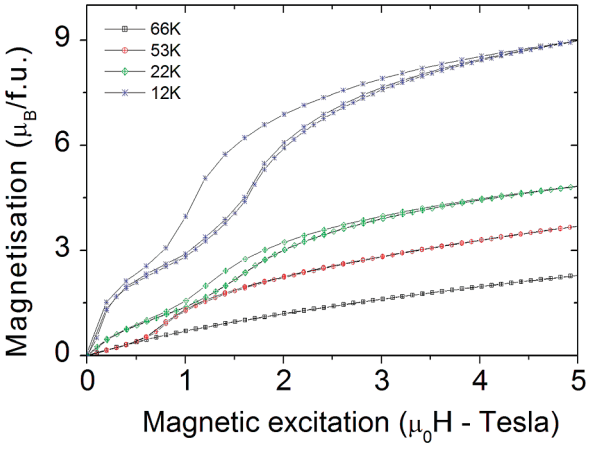

Figure 11. Isothermal Magnetization versus magnetic field at the indicated temperature.

(i) The 3D antiparallel ordering of the 2D units along the c axes, as shown by the Néel-like transition temperature at 56 K for $H = 0.9$ T for $Ba_7Co_6BrO_{17-\delta}$ and from the neutron diffraction data.

(ii) The appearance under high external magnetic field and/or on cooling of a FM-like component as supported by the positive θ_{CW}.

For $Ba_7Co_6BrO_{17-\delta}$, the field-driven-transition suggested by the ND experiments has been analyzed from the isothermal magnetization experiments. A selection of them is shown in Figure 11.

The magnetization loop at 66 K is typical of a paramagnetic behavior. However, no Brillouin law adjusts the experimental data using the average spin state deduced from the effective moment fitted by the Curie−Weiss law (see section IV). Magnetic Short Range Ordering (SRO) likely occurs at such temperature. This is comforted by the enhancement of the low-angle broad diffusion observed in the ND patterns above T_N, characteristic of (intra-block) ferromagnetic short-range correlations. Indeed, similar superparamagnetism as observed in the "parent compound" 2H-$BaCoO_3$[26] could be suggested. Here, magnetic clusters would consist on bunches of linear tetramers already coupled above T_N. It is reminiscent of the 3D-ordering of the related oxo-halides (X = F, Cl) for which similar tetramers/trimers also play the role of magnetic connectors, and order at higher temperature (T_N~110−135 K[12]). We already pointed out a drastic change of the magnetic correlations occurring (from antiparallel to parallel alignment) when H increases. On the isotherm measured at 53 K, a first linear part is shown until 0.5 T as expected from the antiparallel alignment observed along the c-axis from neutron data refinement. This linear evolution is followed by a significant upturn above 0.8 T revealing an order−order magnetic phase transition. No magnetic hysteresis is observed signing a reversible phenomenon. The "critical field" H_c responsible for it is defined as the field for which the fastest change in the

(26) Botta, P. M.; Pardo, V.; Baldomir, D.; de la Calle, C.; Alonso, J. A.; Rivas, J. *Phys. Rev. B* **2006**, *74*, 214415.

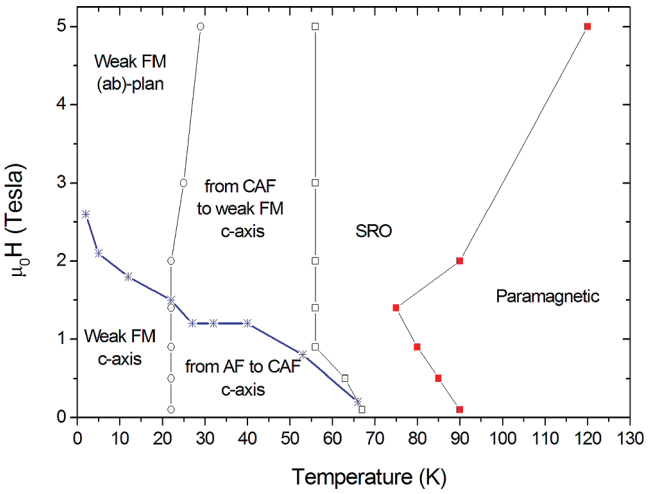

Figure 12. $Ba_7Co_6BrO_{17-\delta}$: Diagram $H-T$ built from the experimental data (temperature dependence of the magnetization and isothermal magnetization versus magnetic field). SRO is a short-range ordering phase ; AF is the antiferromagnetic phase; CAF is a canted antiferromagnetic phase; weak FM is a weak ferromagnetic phase resulting from the spin-flop transition. Solid lines are guides for the eyes.

magnetization occurs. It coincides with a local maximum in the dM/dH curves. Typically, H_c increases significantly when the temperature is lowered, following the continuous loss of the linear part on isothermal $M(H)$ curves at low magnetic field. In fact, the opening of the magnetization loop on the isotherm at 22 K which coincides with the loss of the linear $M(H)$ dependency at low field is already observed at 42 K. Consequently, between ~20 K and 55 K, a field-driven spin flop transition from canted antiferromagnetic to weak ferromagnetic ordering definitively occurs, as characterized by the value of H_c.

Finally, the second sharp transition of $M/H(T)$ around 10 K (see Figures 2 and 9) is assumed to be to a spin-canting phenomenon. It is related to the continuous loss of the linear part on isothermal $M(H)$ curves at low magnetic field. It is highlighted by the small remnant moment observed below 12 K. We already stated that the coinciding spin-tilting at $\mu_0 H = 1.2\ T$ and $T = 1.4$ K could not been refined from our powder ND experiments, even if it is correlated with the low-temperature anomalies shown on the Figure 2.

At this stage, it is worth noting that the value of the first $M(H)$ plateau at 12 K roughly corresponds to one-third of the magnetization at saturation. This behavior is reminiscent of comparable phenomena occurring for related materials such as $Ca_3Co_2O_6$ made of 1D-cobalt Ising chains.[27] In the series of related compounds, such behavior corresponds to the competition between strong in-chain FMs and weaker interchain AFM exchanges. It gives clues for similar effects in $Ba_7Co_6BrO_{17-\delta}$ in which the competition exists between FM blocks containing similar 1D-segments and weaker AFM interblock couplings. In addition, as in $Ca_3Co_2O_6$, it is probable that the exchanges between adjacent tetramers of a same block are negative but dominated by the cooperative FM alignment imposed by the terminal tetrahedral connections.

(27) Kusadov, Y. B., *EuroPhysics Lett.* **2007**, *78*, 5705.

VII. $Ba_7Co_6BrO_{17-\delta}$ Magnetic Phase Diagram

Figure 12 summarizes the final (H,T) phase diagram deduced from the systematic $M(T)$ and $M(H)$ screening of the system combined with analysis of the ND data. The temperature for which the inverse of the magnetic susceptibility and the Curie−Weiss law behavior diverge is correlated to the appearance of short-range ordered (SRO) domains, and it is defined as the disorder/order temperature (full square). Also shown are the long-range antiferromagnetic and weak ferromagnetic ordering temperatures (empty square) related to the magnetic transitions observed on the temperature dependence of the magnetization measured under variable magnetic field, the "critical field" H_c responsible for the spin flop transition at intermediate temperature or the spin reorientation transition at low temperatutre (arrow), and T_{sp} (circle) at which the spin-flop occur. H_c and T_{sp} are defined as the local maximum of dM/dH and as the fastest change on the curvature of the $M(T)$, respectively. As the temperature is lowered, H_c rises up almost linearly until reaching a plateau at 1.2 T in the range 25−40 K. It is worth recalling that $\mu_0 H = 1.2\ T$ corresponds to the value for which a change of magnetic correlation occurs below T_N (see Figure 10). It follows that the divergence of χ^{-1} from the Curie−Weiss law signals the evolution of the field-induced spin flop transition.

For magnetic field lower than 1.2 T, irregular (SRO) occurs above the Néel ordering. Below T_N, the moments align along the c easy axis. Further cooling leads to a continuous transition from AFM to a canted AFM state resulting in an imperfect compensation of the magnetic moment along the c axis. At T_{SP} a spin-flop transition occurs responsible for the second sharp transition on the temperature dependent magnetization and for the opening of the magnetic hysteresis on the isothermal magnetization. The magnetic anisotropy is kept along the c-axis as observed by ND experiment.

For magnetic field greater than 1.2 T, a transition from SRO to canted antiferromagnetic ordering occurs on cooling, responsible for the smoothing of $M(T)$. On further cooling the progressive transition into a weak ferromagnet is signed by the opening of an hysteresis loop which depends on the (H,T) coordinates. For example, the isothermal magnetization at 53 K is perfectly reversible just above H_c while a coercive field of 250 Oe is indeed observed on the isothermal magnetization at 42 K. At lower temperature and for a applied magnetic field larger than H_c, $Ba_7Co_6BrO_{17-\delta}$ likely turns into a weak FM with a net moment in the (ab) plane.

It is clear that the disconnection of the individual blocks by the central $[Ba_2O_{2-\delta}Br]^-$ double-layers enables a competition between various inter and intrablocks exchanges, by comparison to parent $BaCoO_{3-\delta}$ and other oxy-halides polymorphs. A large uniaxial magnetic anisotropy related to the quasi-one-dimensional arrangement of the interacting Co atoms is observed on the 1D- 2H $BaCoO_3$ and gradually lifted from 5H or 12H $BaCoO_{3-\delta}$ to $Ba_7Co_6BrO_{17-\delta}$. In the 5H- $BaCoO_{3-\delta}$ polymorphs

FM exchanges predominate below 50 K and a canted angle of 63° with respect to the *c*-axis was announced.[22] A lowering of the magneto-crystalline anisotropy is supported for strongly disconnected blocks of the two examined $Ba_{n+1}Co_nO_{3n-1}Br$ ($n = 5$ and 6) compounds. The intrablock exchanges have already been extensively discussed for the parent $Ba_6Co_6(Cl, F)O_{16}$.[24,25] Here, a competition between FM metal−metal bonding[24,28] and interblock AFM correlations may also occur. Then the magneto-crystalline anisotropy turns to become of the same order of magnitude than the applied magnetic field which explains such a fascinating (H,T) phase diagram.

VIII. Magnetic Entropy Changes

Figure 13a shows the temperature dependence of the magnetic entropy $\Delta S_M(T,H)$ calculated using the temperature dependence of $(\partial M/\partial T)_H$ determined at $\mu_0 H = 0.9$, 2, and 5*T*, multiplied by the field (see eq 1). Distinct features depending on the temperature and field values are observed. They are analyzed considering the four magnetic phases described in the (H,T) phase diagram.

Let us remember that for FM materials a large peak centered at the Curie temperature is expected whereas a symmetrical-sign-reversed- phenomenon is expected at T_N for AFM materials. When the temperature decreases, $\Delta S_M(T, H = 0.9\ T)$ shows a large distribution of sign. Two different structures are observed. At temperature higher than 40 K, ΔS_M is first positive and then negative at higher temperature. The peak areas are almost symmetric which support the magnetic transition in the antiferromagnetic state at T_N. The second specific feature is the large magnetic entropy change centered at 20 K in association with the smallest one at 5 K. Here, the system changes its arrangement from AFM to a weak ferromagnetic ordering. However, the large dissymmetry between positive and negative $\Delta S_M(T, H = 0.9\ T)$ domains suggests that the spin flop transition is not entirely completed and that some canted spins are still present giving in average a ferrimagnetic-like ordering.[29] Under increasing field, two broad peaks are promoted. The one centered at 25 K is significant of the FM arrangement. The second peak around 64 K at 2 T and 55 K at 5 T is characteristic of the magnetic entropy change due to the spin-flop transition. In summary, the magnetic entropy change is mediated by the competition between the internal magnetic mean field which supports AFM arrangement along the *c* axis and the external applied magnetic field promoting the FM-like spin-flop transition. At 50 K, it results in a field-tuned sign of the magnetic entropy which indicates the possibility of the material being of use as cooling or heating medium depending on the magnetic field amplitude.

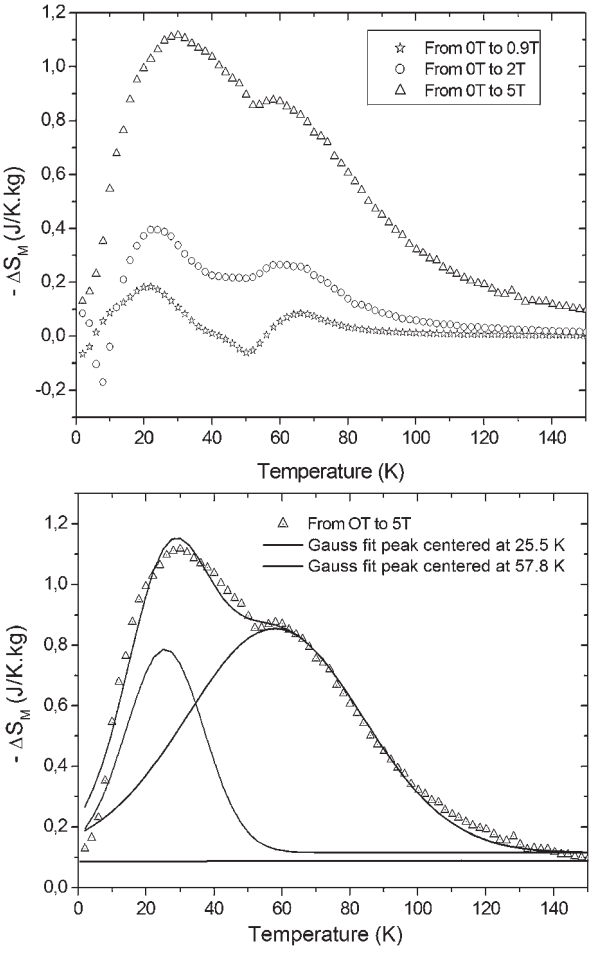

Figure 13. (a) Magnetic entropy change ($-\Delta S_M$) as function of temperature under magnetic field changes deduced from the data presented in Figure 9 and the use of eq 1. (b) The fit of $\Delta S_M(T,5\ T)$ assuming two Gaussian functions centered at 25.5 and 57.8 K.

If one now considers the intrinsic values of the magnetic entropy for $Ba_7Co_6BrO_{17-\delta}$, an average spin value per mole could be obtained from the Curie−Weiss law. A theoretical magnetic entropy of about 10 J/kg K is thus expected using the expression $S_M = R \ln(2S + 1)$. If one sums the maximum magnetic entropy change observed at 60 K and 30 K (0.8 J/kg K and 1.1 J/kg K from Figure 13. a) when 5 T is applied, almost 80% of magnetic entropy is missing. In $Ba_5Co_5O_{14}$, about 50% of the magnetic entropy is missing[22] but this latter displays one canted (*a*,*b*)-plane ferromagnetic phase below 50 K. In contrast, the magnetic entropy for $Ba_7Co_6BrO_{17-\delta}$ is spread out in a wide range of temperature and distributed within at least three phenomena: (i) the short-range ordering, (ii) the spin reorientation, and (iii) the spin-flop transition.

The total refrigerant capacity as defined in section I (equation (3)) is now considered; it is enhanced by the three phenomena. In a first approximation ΔS_M(K, 5 T) is fitted using two Gaussian functions for the entropy due to the spin reorientation and the spin flop respectively over an offset assumed due to the short-range ordering. It allows separating the different contributions of the three phenomena listed before (see Figure 13b). The offset considered before fitting the curve is 0.1 J/kg K. Then the refrigerant capacity of the

(28) Villesuzanne, A.; Whangbo, M.H. *Inorg. Chem.* **2005**, *44*, 6339. Frésard, R.; Laschinger, C.; Kopp, T.; Eyert, V. *Phys. Rev. B* **2004**, *69*, 140405(R).
(29) von Ranke, P. J.; de Oliveira, N. A.; Alho, B. P.; Plaza, E. J. R.; de Sousa, V. S. R.; Caron, L.; Reis, M. S. *J. Phys.: Condens. Matter* **2009**, *21*, 056004.

short-range ordering Q_{SRO} is estimated to 15 J/kg on the temperature range 0−150 K. It is about the same order than the refrigerant capacity due to the spin reorientation transition ($Q_{SP} \sim 19$ J/kg) but three times smaller than $Q_{SR} \sim 48$ J/kg, the refrigerant capacity due to the spin flop transition. As a result that loss of the magnetic entropy in $Ba_7Co_6BrO_{17-\delta}$ is due to the spin flop. Thus, the influence of both the magneto-crystalline anisotropy[30] and of the field induced order/order transition[31] on the magnetocaloric effect is unambiguously shown.

IX. Conclusions

The magnetic phase diagram of $Ba_7Co_6BrO_{17-\delta}$ has been experimentally investigated by neutron diffraction and magnetic measurements. Even if the fundamental magnetic state is an AFM arrangement along the *c* axis, this study shows that an applied magnetic field induces a spin reorientation transition toward the (*a*,*b*) plane, with variable magnitude depending on the temperature. By comparison with the parents layered 5H or 12H-Ba$CoO_{3-\delta}$ hexagonal polytypes, the spin reorientation is explained by a reduction of the magnetocrystalline anistotropy when an extra degree of disconnection between the 2D-blocks is introduced by the $[Ba_2O_2Br]^-$ doublelayers. It enables various magnetic paths between the blocks. A clear competition between the inter-tetrameric blocks antiferromagnetic exchange interaction along the *c* axis J_c and intra-tetrameric blocks ferromagnetic exchange interaction J_{ab} through the (*a*,*b*) plane is suggested. As soon as any magnetic field is applied, the two-dimensional spin-correlations in (*a*,*b*) plane are promoted and a spin flop transition occurs

The second new insight of this study concerns the preponderance of the effect of magnetocrystalline anisotropy on the magnetocaloric properties. It highlights the potentialities of materials with intrinsic multiple magnetic transitions. Of course, efforts are now provided to modify the title compound toward higher temperature transition and local magnetic moments. Here the chemical substitution of iron for cobalt appears promising.

Acknowledgment. O.T. and O.I. acknowledge the "Programme Interdisciplinaire ENERGIE" of CNRS (France) for financial support. Laboratoire Leon Brillouin (LLB), Saclay, France and Institut Laue-Langevin (ILL), Grenoble, France are acknowledged for providing neutrons facilities.

(30) Reis, M. S.; Rubinger, R. M.; Sobolev, N. A.; Valente, M. A.; Yamada, K.; Sato, K.; Todate, Y.; Bouravleuv, A.; Von Ranke, P. J.; Gama, S. *Phys. Rev. B* **2008**, *77*, 104439.
(31) Samanta, T.; Das ans, I.; Banerjee, S. *Appl. Phys. Lett.* **2007**, *91*, 082511.